Smart Structures and Systems, *Vol. 25, No. 3 (2020) 311-322*
DOI: https://doi.org/10.12989/sss.2020.25.3.311

Parametric study of SMA helical spring braces for the seismic resistance of a frame structure

Jincheng Ding, Bin Huang*, Hongwang Lv and Hongxia Wan

School of Civil Engineering and Architecture, Wuhan University of Technology,
122 Luoshi Road, Hongshan District, Wuhan, Hubei Province, China

(*Received October 3, 2019, Revised December 4, 2019, Accepted December 31, 2019*)

Abstract. This paper studies the influence of parameters of a novel SMA helical spring energy dissipation brace on the seismic resistance of a frame structure. The force-displacement relationship of the SMA springs is established mathematically based on a multilinear constitutive model of the SMA material. Four SMA helical springs are fabricated, and the force-displacement relationship curves of the SMA springs are obtained via tension tests. A numerical dynamic model of a two-floor frame with spring energy dissipation braces is constructed and evaluated via vibration table tests. Then, two spring parameters, namely, the ratio of the helical spring diameter to the wire diameter and the pre-stretch length, are selected to investigate their influences on the seismic responses of the frame structure. The simulation results demonstrate that the optimal ratio of the helical spring diameter to the wire diameter can be found to minimize the absolute acceleration and the relative displacement of the frame structure. Meanwhile, if the pre-stretch length is assigned a suitable value, excellent vibration reduction performance can be realized. Compared with the frame structure without braces, the frames with spring braces exhibit highly satisfactory seismic resistance performance under various earthquake waves. However, it is necessary to select an SMA spring with optimal parameters for realizing optimal vibration reduction performance.

Keywords: dissipation brace; Shape memory alloy(SMA); frame structure; parametric study; vibration test; seismic response

1. Introduction

In recent decades, structural integrity assurance and disaster mitigation have received substantial attention in civil engineering, for which two main approaches are utilized: One approach is to use structural health monitoring (Casciati and Wu 2012, An *et al*. 2014, Zhou *et al*. 2019) to issue an early warning if structural damages or deficiencies are identified so that repair or retrofitting can be performed timely (Song *et al*. 2006b). The other approach is to use structural vibration control (Huang *et al*. 2018a, Wang *et al*. 2018a) to enhance the performance of structures in withstanding disasters such as earthquakes and hurricanes. The use of energy-dissipating members or devices in a structure can effectively consume vibration energy inputs to the structure from external excitations, such as earthquakes, strong winds, and impacts (Yang *et al*. 2017, Hayashi *et al*. 2018). Via this mechanism, the energy-dissipating members can rapidly reduce the vibrational responses of the structure. Therefore, the energy-dissipating members can be used to protect the main structure from such external excitations (Zhang *et al*. 2012, Yoshida and Dyke 2004). As a result, energy-dissipation technology has received substantial attention in structural vibration control (Sun 2011, De Domenico and Ricciardi 2018). Various new types of energy dissipating devices, such as eddy current dampers (Bae *et al*. 2005), viscoelastic dampers (Kim and Ryu 2006, Wang *et al*. 2019), and pounding tuned mass dampers (Wang *et al*. 2018b), have been developed (Zapateiro *et al*. 2009, Friedman *et al*. 2013). In recent decades, the application of smart materials to vibration control and shock absorption has become a new development direction (Saadat *et al*. 2002, Gu and Song 2007). Among various smart materials, due to their unique mechanical properties, shape memory alloys have been used to dissipate the input energy of structures in earthquakes and under other types of excitations in recent years (Casciati *et al*. 2007).

Shape memory alloys are a class of smart materials that have a memory function on the shape (Song *et al*. 2006a, Casciati and Faravelli 2009, Casciati and van der Eijk 2008). Their most unique properties are shape memory and superelasticity (Xu and Song 2004, Qian *et al*. 2016). Superelasticity offers energy dissipation (Song *et al*. 2004). The energy consumption performance of the SMA material renders it suitable for energy dissipation control (Ren *et al*. 2007, Patil and Song 2016). The use of SMA helical springs to control structural vibration has recently attracted researchers' attention. Huang *et al*. (2014) used the SMA springs as base isolators to protect a structure from an earthquake. Mishra *et al*. (2013) studied the seismic responses of a structure with a tuned mass damper (TMD) that was facilitated by SMA helical springs and discussed

*Corresponding author, Professor,
E-mail: binhuang@whut.edu.cn

http://www.techno-press.org/?journal=sss&subpage=7
ISSN: 1738-1584 (Print), 1738-1991 (Online)

the vibration reduction performance of the improved TMD. Using SMA helical springs as braces, Huang *et al*. (2018b) proposed a new frame structure for resisting earthquakes, and both experimental and numerical results demonstrated the satisfactory performance of SMA spring braces. Since the earthquake is a kind of random reciprocating load, the fatigue analysis of the SMA springs needs to be considered. Many researchers have implemented a lot of significant studies on this aspect (Carreras *et al*. 2010, Sedlák *et al*. 2013, Casciati *et al*. 2016, Kundu *et al*. 2018, Hashemi *et al*. 2019). Regarding that the earthquake seldom happens in the same place for many times and the lasting time of one earthquake is usually short, the fatigue problem of the SMA springs will not be discussed in this paper.

Based on a study that was implemented in the literature (Huang *et al*. 2018b, 2019), this paper mainly studies the influence of the parameters of the helical spring in the energy dissipation brace on the seismic resistance of the frame structure. The influences of two spring parameters, namely, the ratio of the helical spring diameter to the wire diameter and the pre-stretch length, on the seismic responses of the frame structure are investigated. To complete this study, four SMA springs are fabricated, and the force-displacement relationship curve of the SMA springs is generated. A numerical dynamic model of a two-floor frame with the spring energy dissipation braces is constructed and evaluated via vibration table tests.

2. Mechanical model of an SMA helical spring

2.1 Constitutive model of SMA material

Boyd and Lagoudas (1996) proposed a thermodynamic multilinear model and Motahari and Ghassemieh (2007) modified it. The proposed model simulates the performance of SMA under seismic applications accurately. There are two types of SMA crystallographic phases: austenite and martensite. It is possible to convert between the two phases via temperature or stress change. A schematic diagram of the constitutive model, or the stress-strain relationship, of a superelastic SMA is shown in Fig. 1, where B, C, E and F are called the martensite start point, the martensite finish temperature, the austenite start point and the austenite finish point, respectively. Their corresponding stresses are σ_{Ms}, σ_{Mf}, σ_{As} and σ_{Af}, respectively. Their corresponding strains are ε_{Ms}, ε_{Mf}, ε_{As} and ε_{Af}, respectively.

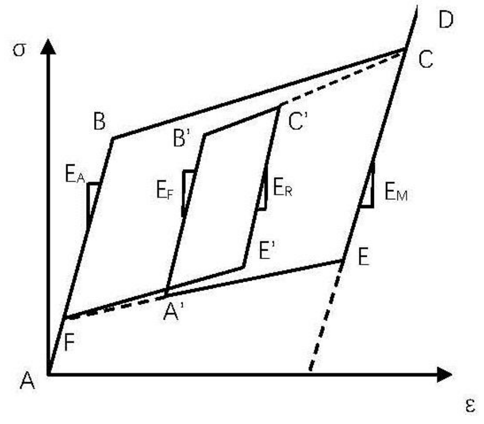

Fig. 1 Schematic diagram of the multilinear constitutive model

The multilinear stress–strain relations in Fig. 1 can be represented by the following formulas, which are related to multi-paths:

Paths A-B and F-A

$$\sigma = E_A \varepsilon \tag{1}$$

Path B-C

$$\sigma = \sigma_{M_s} + \frac{\varepsilon - \varepsilon_{M_s}}{\varepsilon_{M_f} - \varepsilon_{M_S}}\left(\sigma_{M_f} - \sigma_{M_S}\right) \tag{2}$$

Paths C-D and D-E

$$\sigma = \sigma_{M_f} + E_M(\varepsilon - \varepsilon_{M_f}) \tag{3}$$

Path E-F

$$\sigma = \sigma_{A_s} + \frac{\varepsilon - \varepsilon_{A_s}}{\varepsilon_{A_f} - \varepsilon_{A_S}}\left(\sigma_{A_f} - \sigma_{A_S}\right) \tag{4}$$

where E_A and E_M are the elastic moduli of austenite and martensite, respectively.

If the loading occurs during the unloading process, or the unloading occurs during the loading process, new values of stress and strain can be determined using the previous unloading or loading points. The curve A′-B′-C′-E′ in Fig. 1 describes the constitutive model of the subloop. The elastic moduli of the SMA on the paths A′-B′ and C′-E′ can be represented as

$$E_i(\xi) = \frac{E_M E_A}{\xi(E_A - E_M) + E_M}(i = F, R) \tag{5}$$

where ξ is the martensite volume fraction.

The strain values at the points B′ and E′ in the subloop can be written as follows

$$\varepsilon'_{M_s} = \varepsilon'_{min} + \frac{\sigma_{M_s} - \sigma'_{min}}{E_F} \tag{6}$$

$$\varepsilon'_{A_s} = \varepsilon'_{max} + \frac{\varepsilon_{A_s} - \varepsilon'_{max}}{E_R} \tag{7}$$

where σ'_{min} and σ'_{max} are the minimum and the maximum stresses, respectively, in the subloop; ε'_{min} and ε'_{max} are the minimum and maximum strains, respectively, in the subloop. Following Eqs. (5)-(7), the stress-strain relationship of the SMA related to the subloop can be determined.

Since the experimental shear stress-strain curve of the SMA wire was found to be similar to the tensile stress-strain curve that is obtained above, the presented constitutive model can be used to demonstrate the shear stress-strain relationship of the SMA wire. Hence, the normal stress, normal strain and elastic modulus in the Eqs. (1)-(4) and the

Eqs. (6)-(7) can be replaced by the shear stress, shear strain and shear modulus, respectively.

2.2 Force-displacement relationship of the SMA helical spring

Now let us consider a helical spring that is made of SMA wire and is subjected to an axial load *F*. Suppose that the torsional deformation occurs uniformly on the cross-section of the wire and the shear strain linearly changes along the radius. Then, the shear strain γ at a point on the cross-section of the SMA wire can be expressed as (Aguiar *et al*. 2010)

$$\gamma(\mathrm{r}) = \frac{2r}{\pi D^2 N} \cdot u \tag{8}$$

where *u*, *r*, *D* and *N* are the axial displacement of the spring, the radial coordinate of a point relative to the center of the wire, the diameter of the spring and the number of coils, respectively.

Based on the equilibrium of torsional moment of the SMA helical spring, the equilibrium equation can be expressed as follows

$$\mathrm{FD} = 4\pi \int_0^d \tau r^2 dr \tag{9}$$

where τ is the shear stress at the radial coordinate *r* on the cross-section of the wire, which can be obtained from the shear stress-strain relationship, and *d* is the wire radius. The force-displacement relationship of the SMA spring under a seismic load can be obtained by following the steps that are described above.

(a) SMA helical spring

Fig. 3 Tensile test of an SMA l

It is worth mention that the constitutive model of the SMA used in this paper does not involve in the strain rate since the inpaction of the strain rate on the force-displacement relationship of the SMA helical spring is not large (Ren *et al*. 2007, Enemark *et al*. 2016).

3. Tensile tests of the SMA helical spring

In this paper, the most commonly applied nickel-titanium (Ni-Ti) alloy wire is used to make the helical spring. The Ni-Ti alloy wire that is used for the test was supplied by Jiangyin Falsun Pell New Material Technology Co., Ltd. The Ni-Ti alloy wire has a Ni metal content of 50.8%. The material is in an austenitic state at room temperature. Two kinds of SMA wires are used in this paper, whose diameters are 1 mm and 0.8 mm, respectively. For the wire with the diameter of 1 mm, the temperature at the end of the austenitic transformation is -29°C. And for another one, the temperatures at the end of the austenitic transformation is -14°C.

(a) Type I (D = 8, d = 1) (b) Type II (D = 10, d = 1) (c) Type III (D = 10, d = 0.8) (d) Type IV (D = 12, d = 0.8)

Fig. 2 SMA helical springs with various geometrical parameters

Since the fabrication technique has a strong influence on the hysteretic behavior of the SMA helical spring, it is necessary to find a suitable heating temperature, heating time and cooling method such that the SMA helical spring has a satisfactory superelastic property. In this paper, based on previous research, the SMA helical spring is trained via thermal processing. During the thermal processing, one SMA wire is wrapped around a threaded rod to form the spring and is held in an oven at 450°C for 30 minutes. After

Table 1 Physical parameters of the SMA material and the geometric parameters of the springs

Parameter	Type I	Type II	Type III	Type IV
D (mm)	8	10	10	12
d (mm)	1	1	0.8	0.8
G_A (GPa)	25.3	21	30	28
G_M (GPa)	25	20	29	27
τ_{Ms} (MPa)	156.6	124	208	161
τ_{Mf} (MPa)	394.2	292	819	759
τ_{As} (MPa)	151.2	120	169	149.5
τ_{Af} (MPa)	16.2	12	39	34.5
γ_{Ms} (%)	6.19	6.11	6.86	5.75
γ_{Mf} (%)	40.77	39.6	52.3	53.1
γ_{As} (%)	31.05	31	30.57	30.53
γ_{Af} (%)	0.64	0.59	1.29	1.23

that, the spring is cooled in water.

Following the fabrication steps that are described in the above section, an SMA spring can be trained. In this study, four type of springs were manufactured, as shown in Fig. 2. The mechanical parameters of the four springs are listed in Table 1. Using the listed parameters and Eqs. (1)-(9), the force-displacement relationships of the springs can be simulated numerically. Meanwhile, a series of tensile tests on the four springs, which are shown in Fig. 3, are conducted. Via this approach, the force-displacement curves of the SMA springs can be obtained experimentally and are plotted in Fig. 4. Fig. 4 shows that the simulated force-displacement curves accord with the tested force-displacement curves. From Figs. 4(a)-(b), it is found that when the load surpasses 22 N and 14 N, respectively, the quick up trend of the force-displacement curves appears for the Type I and II springs. This is attributed to that under those loads, the shear stress on the cross section of the SMA wires exceeds the value of τ_{Mf}, which is the critical shear stress at the end of the martensitic transformation.

4. Dynamic simulation and vibration test of a frame with SMA spring braces

4.1 Simulation model of the frame structure system

The proposed energy dissipation brace is composed of a trained SMA spring and two steel bars. A two-floor steel frame model is established for studying the dynamic responses of a frame structure that is equipped with the proposed energy dissipation braces. Fig. 5 illustrates the configuration of the frame structure. The model assumes that the beam stiffness is much larger than the stiffness of the two columns, and the axial deformation of the beam and the columns is neglected. The two beams are simplified as two concentrated mass points so that the frame becomes a two-degree-of-freedom system.

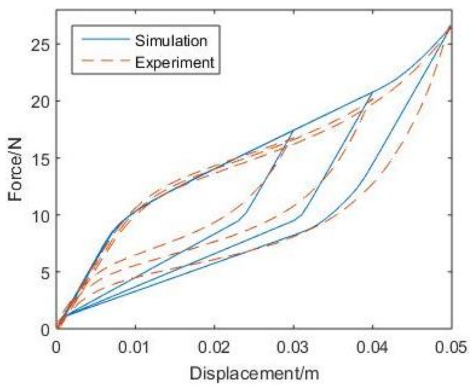

(a) Type I

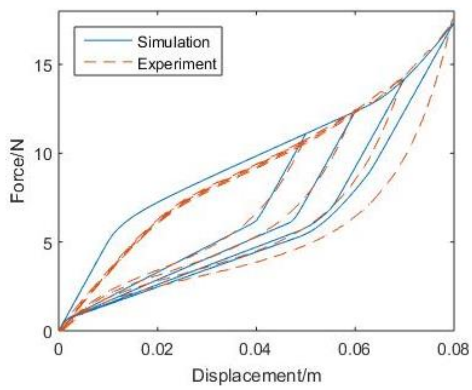

(b) Type II

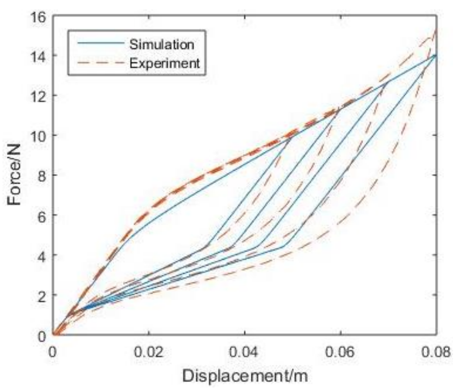

(c) Type III

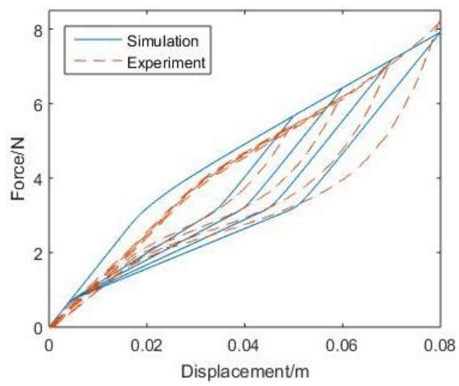

(d) Type IV

Fig. 4 Simulated and experimental force-displacement curves of the four springs

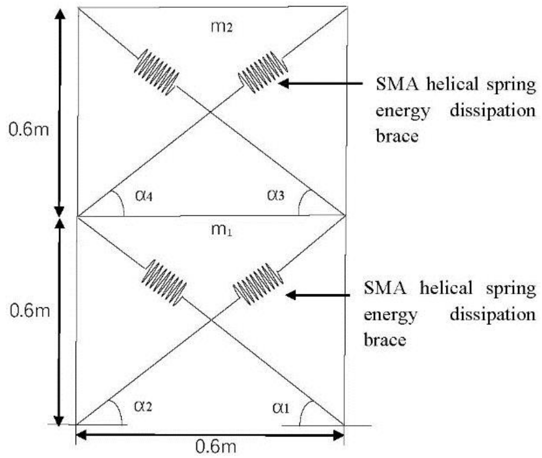

Fig. 5 Configuration of the frame structure

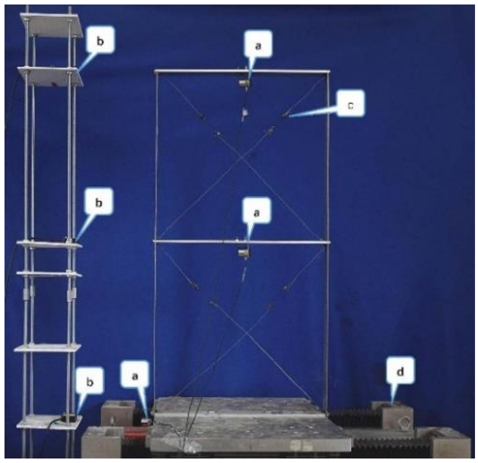

Fig. 6 Two-floor steel frame model
(a = acceleration sensors; b = laser displacement sensors; c = vibration table; and d = SMA spring brace)

4.2 Dynamic equation of the frame model

Based on the mechanical model of the frame in Section 4.1, the dynamic equation of the structure under seismic excitation can be expressed as follows

$$M\ddot{U} + C\dot{U} + KU = -M\{I\}\ddot{x}_g + F \tag{10}$$

Where

$$\mathrm{M} = \begin{bmatrix} m_1 & 0 \\ 0 & m_2 \end{bmatrix} \tag{11}$$

$$\mathrm{C} = a_0 M + a_1 K \tag{12}$$

$$\mathrm{K} = \begin{bmatrix} k_1 + k_2 & -k_2 \\ -k_2 & k_2 \end{bmatrix} \tag{13}$$

$$\mathrm{U} = \begin{bmatrix} u_1 \\ u_2 \end{bmatrix} \tag{14}$$

$$\begin{bmatrix} a_0 \\ a_1 \end{bmatrix} = 2\frac{\omega_1\omega_2}{\omega_2^2 - \omega_1^2}\begin{bmatrix} \omega_2 & -\omega_1 \\ -{}^{1}/_{\omega_2} & {}^{1}/_{\omega_1} \end{bmatrix}\begin{bmatrix} \xi_1 \\ \xi_2 \end{bmatrix} \tag{15}$$

$$\mathrm{F} = \begin{bmatrix} F_1 cos\alpha_1 - F_2 cos\alpha_2 + F_4 cos\alpha_4 - F_3 cos\alpha_3 \\ F_3 cos\alpha_3 - F_4 cos\alpha_4 \end{bmatrix} \tag{16}$$

where u_1 and u_2 are the relative displacements of the first and second floors, respectively; m_1 and m_2 are the mass values of the first and second layers of the frame, respectively; k_1 and k_2 are the horizontal stiffness values of the first and second layers, respectively; α_i (i = 1, 2, 3, 4) is the angle between the horizontal beam and the ith energy dissipation brace; F_i (i = 1, 2, 3, 4) is the axial force of the ith energy dissipation brace; ω_1 and ω_2 are the first and second frequencies, respectively, of the two-floor frame model; ξ_1 and ξ_2 are the first and second modal damping ratios, respectively, of the frame; and $\ddot{x}_g$ is the earthquake acceleration input in the horizontal direction.

4.3 Vibration experiment on the frame structure

A two-floor steel frame model was produced according to the simulation model in Section 4.1, as shown in Fig. 6. Via measurement and calculation, it is determined that the mass m_1 of the first layer is 2.40 kg and the mass m_2 of the second layer is 1.72 kg. The lateral stiffness k_1 of the first layer is 1630 N/m, and the lateral stiffness k_2 of the second layer is 1890 N/m. In addition, the damping ratio of the frame structure is determined via the free vibration attenuation method. The values of ξ_1 and ξ_2 are 0.00286 and 0.00313, respectively. The four SMA springs in the energy dissipation brace are the same, and they can be any type among the trained four types of springs, whose parameters are shown in Table 1.

4.4 Comparison of the simulated dynamic responses with the experimental results

To explore the vibration reduction performance of the proposed SMA spring brace, this paper studied the following two types of scenarios: (1) No control: no brace component is installed in the frame; and (2) the SMA spring brace is installed. The spring that is used in the brace is a Type II spring, and the pre-stretch length is 70 mm. First, in the frequency domain, the relative displacement amplitudes of the second floor are simulated, where the acceleration amplitude of input simple harmonic waves is 0.1 g. Fig. 7

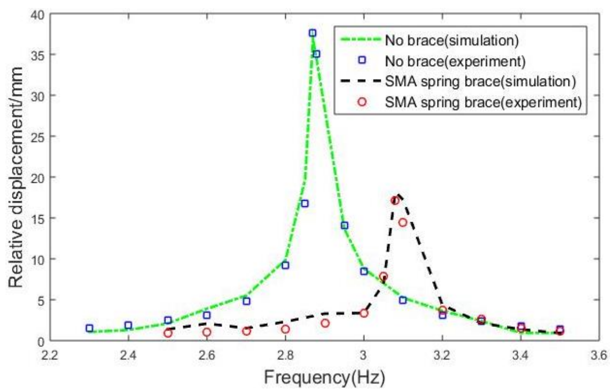

Fig. 7 Relative displacement response of the second floor of the frame under excitations of varying frequencies

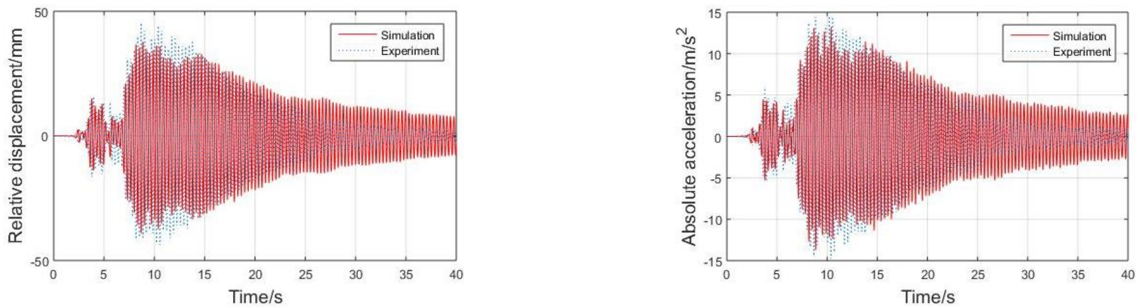

(a) Relative displacement (b) Absolute acceleration

Fig. 8 Numerical and experimental responses of the frame for the Kobe wave (no brace)

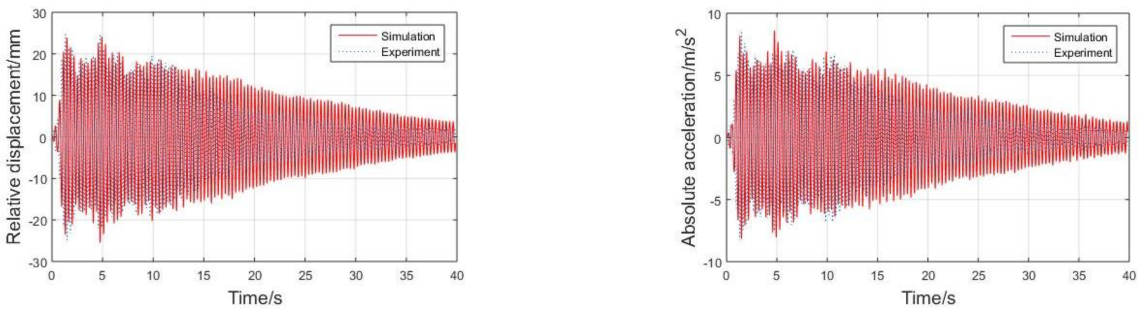

(a) Relative displacement (b) Absolute acceleration

Fig. 9 Numerical and experimental responses of the frame for the Hollister wave (no brace)

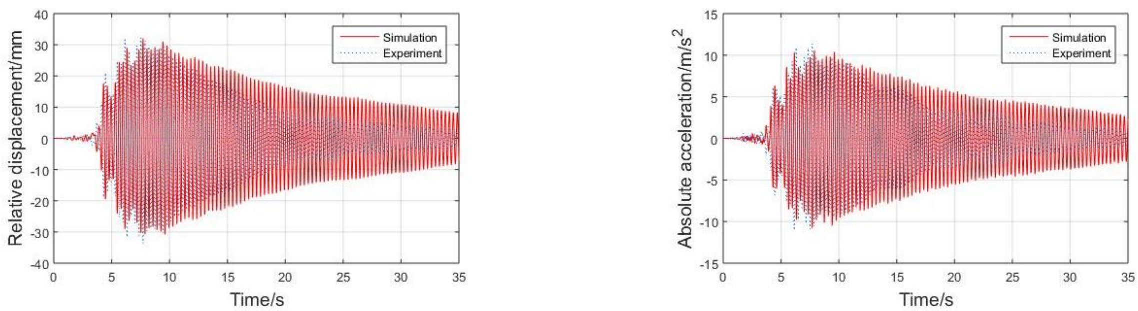

(a) Relative displacement (b) Absolute acceleration

Fig. 10 Numerical and experimental responses of the frame for the Friuli wave (no brace)

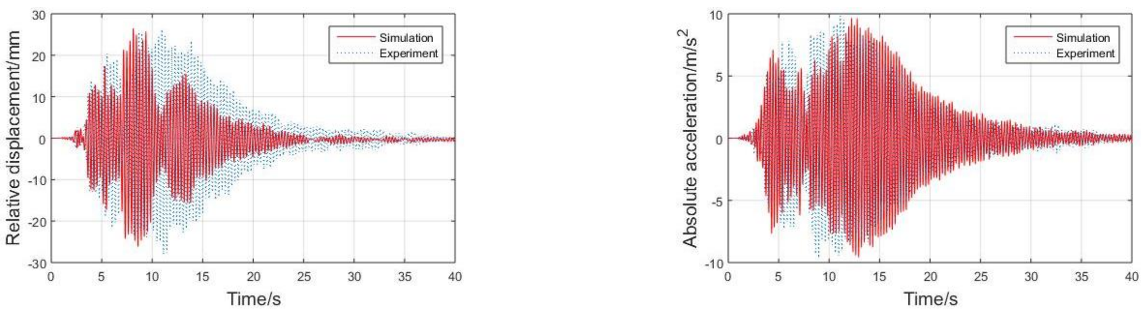

(a) Relative displacement (b) Absolute acceleration

Fig. 11 Numerical and experimental responses of the frame for the Kobe wave (SMA spring brace)

plots the simulated and experimental displacements of the second floor of the frame under excitations of varying frequencies. From Fig. 7, the simulated relative displacements accord with the experimental results, which demonstrates the satisfactory performance of the simulation model of the frame with or without braces. In addition, the

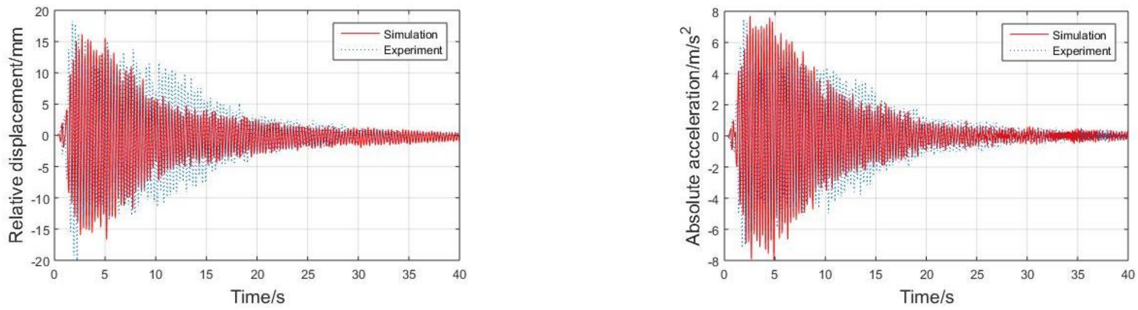

(a) Relative displacement (b) Absolute acceleration

Fig. 12 Numerical and experimental responses of the frame for the Hollister wave (SMA spring brace)

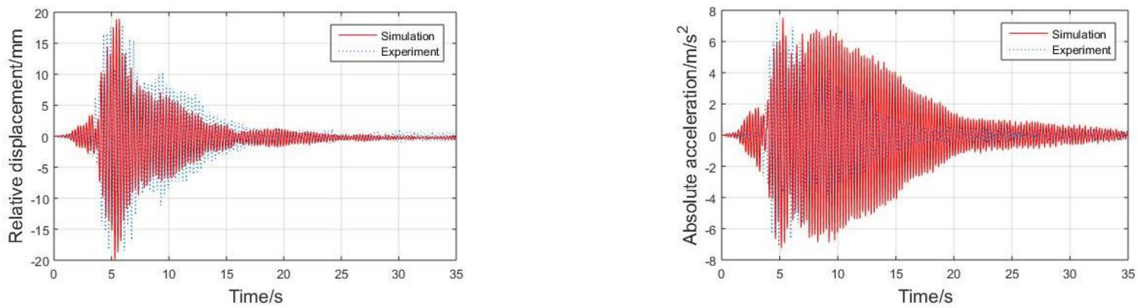

(a) Relative displacement (b) Absolute acceleration

Fig. 13 Numerical and experimental responses of the frame for the Friuli wave (SMA spring brace)

Table 2 Relative errors of the simulated peak seismic responses to the corresponding experimental results for two cases

Case	Seismic responses	Hollister wave (%)	Kobe wave (%)	Friuli wave (%)
No brace	Relative displacement	1.16	16.55	0.62
	Absolute acceleration	2.04	13.22	7.02
SMA spring brace	Relative displacement	12.20	3.75	5.34
	Absolute acceleration	3.53	2.05	4.63

resonant frequency of the frame with braces is larger than that of the frame without braces, and the peak response of the frame with braces is far weaker than that of the frame without braces. Thus, the braces substantially reduce the dynamic responses of the frame.

To study the seismic responses of the frame structure with the braces, three earthquake waves, namely, the Hollister wave, the Kobe wave and the Friuli wave, are chosen. The peak ground acceleration (PGA) of the earthquake waves was 0.2 g. Figs. 8-13 compares the simulated responses with the experimental results of the frame with and without braces under various earthquake waves. In Figs. 8-13, the relative displacement and the absolute acceleration of the second floor are plotted. According to Figs. 8-13, the simulated peak responses accord with the experimental results. The relative errors of the numerical peak responses to the experimental peak responses are listed in Table 2. According to Table 2, the relative errors are very small; hence, the simulated dynamic model is highly useful for the parameter analysis of the springs.

5. Parameter study

To obtain a rational design of the SMA spring brace, the effects of the ratio of the helical spring diameter to the wire diameter and the pre-stretch length are studied. Four types of SMA springs, namely, the Type I, II, III and IV springs, are selected as the spring braces. Three earthquake waves, namely, the Kobe wave, the Hollister wave and the Friuli wave, are considered.

5.1 Impact of the ratio of the helical spring diameter to the wire diameter

The ratio of the helical spring diameter to the wire diameter is an important spring parameter, which is denoted as Rsw in this paper. The index Rsw affects the stiffness of the SMA spring and influences the seismic performance of the energy dissipation brace. The Rsw values of the Type I, II, III and IV springs are 8, 10, 12.5 and 15, respectively. The lower the value of Rsw, the higher the stiffness of the spring.

This paper studied the reduction ratios of seismic responses of the frame with the helical SMA spring braces while being subjected to the three earthquake waves. Here,

Table 3 Vibration reduction ratios under the same pre-stretch length (the pre-stretch length is 50 mm)

R_{sw}	Seismic wave (0.2 g PGA)	Absolute acceleration of the 1st floor (%)	Relative displacement of the 1st floor (%)	Absolute acceleration of the 2nd floor (%)	Relative displacement of the 2nd floor (%)
8	Kobe wave	42.96 (38.51)	61.32 (60.45)	50.66 (44.56)	63.27 (59.93)
10		16.07 (22.42)	44.27 (41.27)	23.66 (28.71)	53.94 (41.25)
12.5		8.17	30.82	27.76	28.97
15		2.64	1.79	5.34	2.35
8	Hollister wave	15.15 (10.28)	41.29 (40.37)	14.26 (11.81)	42.85 (40.93)
10		5.15 (11.50)	28.31 (22.82)	5.97 (13.19)	28.91 (23.66)
12.5		12.36	14.68	9.54	16.42
15		10.26	8.23	5.36	5.83
8	Friuli wave	39.66 (35.86)	50.24 (49.51)	35.62 (34.48)	50.63 (50.84)
10		30.67 (29.48)	47.84 (33.68)	27.01 (34.48)	42.20 (38.53)
12.5		5.38	5.53	16.67	12.06
15		3.30	0.91	3.87	6.98

Table 4 Vibration reduction ratios under the same ratio of the helical spring diameter to the wire diameter (R_{sw} is 8)

Pre-stretch length (mm)	Seismic wave (0.2 g PGA)	Absolute acceleration of the 1st floor (%)	Relative displacement of the 1st floor (%)	Absolute acceleration of the 2nd floor (%)	Relative displacement of the 2nd floor (%)
30	Kobe wave	45.95 (43.88)	63.18 (62.55)	51.21 (49.80)	64.14 (63.28)
40		43.26 (40.45)	61.02 (62.21)	51.19 (48.64)	64.10 (61.97)
50		42.96 (38.51)	61.32 (60.45)	50.66 (44.56)	63.27 (59.93)
30	Hollister wave	16.31 (17.42)	42.31 (40.64)	15.86 (16.32)	42.77 (42.64)
40		15.95 (12.37)	41.44 (42.89)	15.48 (16.20)	43.02 (42.10)
50		15.15 (10.28)	41.29 (40.37)	14.26 (11.81)	42.85 (40.93)
30	Friuli wave	40.27 (39.97)	51.21 (50.54)	36.19 (37.32)	51.24 (51.15)
40		39.89 (39.44)	50.67 (50.63)	35.83 (35.00)	51.37 (50.93)
50		39.66 (35.86)	50.24 (49.51)	35.62 (34.48)	50.63 (50.84)

Table 5 Vibration reduction ratios under the same ratio of the helical spring diameter to the wire diameter (R_{sw} is 10)

Pre-stretch length (mm)	Seismic wave (0.2 g PGA)	Absolute acceleration of the 1st floor (%)	Relative displacement of the 1st floor (%)	Absolute acceleration of the 2nd floor (%)	Relative displacement of the 2nd floor (%)
30	Kobe wave	15.19	42.94	22.18	53.14
40		16.92	43.91	23.27	53.27
50		16.07 (22.42)	44.27 (41.27)	23.66 (28.71)	53.94 (41.15)
60		14.71 (22.75)	44.40 (39.87)	23.81 (28.64)	54.70 (42.56)
70		15.45 (19.53)	44.84 (41.37)	23.51 (31.63)	54.38 (42.01)
30	Hollister wave	3.91	27.60	5.06	28.65
40		4.43	28.09	5.33	28.37
50		5.15 (11.50)	28.31 (22.82)	5.97 (13.19)	28.91 (23.66)
60		5.44 (11.32)	28.14 (25.98)	6.22 (11.46)	29.05 (24.48)
70		5.95 (12.71)	28.42 (25.52)	6.94 (12.62)	29.43 (26.16)
30	Friuli wave	30.02	47.26	26.84	42.37
40		30.69	47.91	25.99	42.61
50		30.67 (29.48)	47.84 (33.68)	27.01 (34.48)	42.20 (38.53)
60		32.67 (35.19)	48.74 (39.97)	28.17 (35.77)	42.78 (39.72)
70		33.95 (38.78)	50.67 (42.98)	28.39 (36.89)	43.96 (43.54)

the reduction ratio refers to the relative percentage error between the peak response in the no-brace case and that in the SMA spring brace case. Table 3 lists the reduction ratios of the seismic responses that were obtained via numerical simulations. In Table 3, the results in parentheses are the partial tested reduction ratios. According to Table 3, the simulated reduction ratios accord with the experimental results, which further demonstrates that the obtained reduction ratios are effective. Moreover, as the value of R_{sw} increases, the reduction ratio decreases under the three earthquake waves. When the pre-stretch length is the same, the optimal R_{sw} is 8 among the four SMA springs for maximizing the reduction ratio.

5.2 Impact of the pre-stretch length

In this section, the influence of the pre-stretch length of the SMA springs on the seismic responses is studied. The pre-stretch lengths of the Type II and Type III springs in the vibration tests are 30 mm, 40 mm, 50 mm, 60 mm and 70 mm. For the Type I spring, R_{sw} is so small that the maximum pre-stretch length of the spring is only 50 mm.

To investigate the impact of the pre-stretch length of the SMA springs on the seismic responses, the three earthquake

Table 6 Vibration reduction ratios under the same ratio of the helical spring diameter to the wire diameter (R_{sw} is 12.5)

Pre-stretch length (mm)	Seismic wave (0.2 g PGA)	Absolute acceleration of the 1st floor (%)	Relative displacement of the 1st floor (%)	Absolute acceleration of the 2nd floor (%)	Relative displacement of the 2nd floor (%)
30	Kobe wave	8.55	30.81	28.18	29.84
40		8.31	30.05	27.92	29.27
50		8.17	30.82	27.76	28.97
60		7.37 (6.76)	29.43 (23.33)	27.28 (24.01)	28.04 (24.74)
70		7.95 (8.37)	29.42 (22.57)	27.09 (25.10)	28.48 (24.79)
30	Hollister wave	12.82	13.27	9.37	15.67
40		12.27	13.36	9.64	16.38
50		12.36	14.68	9.54	16.42
60		12.93 (5.75)	14.03 (9.04)	9.98 (9.38)	17.32 (9.87)
70		13.35 (13.76)	15.47 (12.72)	10.25 (5.67)	17.84 (10.88)
30	Friuli wave	4.71	4.92	15.36	11.35
40		5.01	5.01	15.91	12.15
50		5.38	5.53	16.67	12.06
60		5.25 (2.79)	5.34 (5.99)	16.92 (12.90)	12.22(7.53)
70		5.08 (4.25)	5.9 (5.95)	18.96 (1..41)	12.27 (8.81)

Table 7 Vibration reduction ratios under the same ratio of the helical spring diameter to the wire diameter (R_{sw} is 15)

Pre-stretch length (mm)	Seismic wave (0.2 g PGA)	Absolute acceleration of the 1st floor (%)	Relative displacement of the 1st floor (%)	Absolute acceleration of the 2nd floor (%)	Relative displacement of the 2nd floor (%)
30	Kobe wave	1.39	0.77	6.37	2.99
40		2.19	1.83	5.60	2.76
50		2.64	1.79	5.34	2.35
60		2.42 (-6.65)	1.39 (7.83)	4.33 (1.58)	1.57 (4.79)
70		2.82 (-8.75)	0.38 (3.88)	2.94 (-5.05)	1.34 (3.87)
30	Hollister wave	10.94	8.82	4.69	5.37
40		10.39	8.91	4.81	5.08
50		10.26	8.23	5.36	5.83
60		9.49 (5.75)	8.36 (4.15)	5.76 (2.43)	6.24 (4.03)
70		9.24 (10.98)	7.36(6.26)	6.04 (2.55)	6.61 (6.68)
30	Friuli wave	2.35	0.47	4.66	5.08
40		2.96	0.26	4.31	6.61
50		3.30	0.91	3.87	6.98
60		3.28 (-2.66)	1.13 (0.49)	4.24 (5.50)	6.82 (1.95)
70		2.83 (-0.66)	1.37 (2.26)	5.37 (8.34)	7.27 (3.44)

waves are used to obtain the reduction ratios. The PGA of all earthquake waves is 0.2 g. Tables 4-7 list the reduction ratios of the seismic responses of the frame with various springs, which are obtained by dynamic simulations. In these tables, the results in the parenthesis are the partial experimental reduction ratios. According to Tables 4-7, the simulated reduction ratios accord with the experimental results.

From Table 4, the optimal pre-stretch length is 30 mm for realizing a satisfactory reduction ratio for the Type I spring. For the Type II spring, according to Table 5, the optimal pre-stretch length is 70 mm for the three earthquake waves. For the Type III spring, according to Table 6, for the Kobe wave, the Hollister wave and the Friuli wave, when the pre-stretch lengths of the SMA spring are 30 mm, 70 mm and 70 mm, respectively, the reduction ratios are the largest. For the Type IV spring, the reduction ratio for each earthquake wave is the largest when the pre-stretch lengths are 30 mm, 70 mm and 70 mm, respectively. In summary, these results demonstrate that for various SMA springs, the optimal pre-stretch length is difficult to realize. However, when the pre-stretch length is suitable, highly satisfactory vibration reduction performance can be realized.

According to the parametric study of the four types of SMA spring braces, the optimal values of the two parameters, namely, the ratio of the helical spring diameter to the wire diameter and the pre-stretch length, can be determined for the seismic resistance of the frame. Finally, Type I spring is selected as a result of the optimization. When the pre-stretch length of the spring is 30 mm, the seismic responses of the frame with the SMA spring braces are calculated in the case of the three earthquake waves. The PGAs of the earthquake waves are assumed to be 0.2 g. The response histories of the second floor of the frame

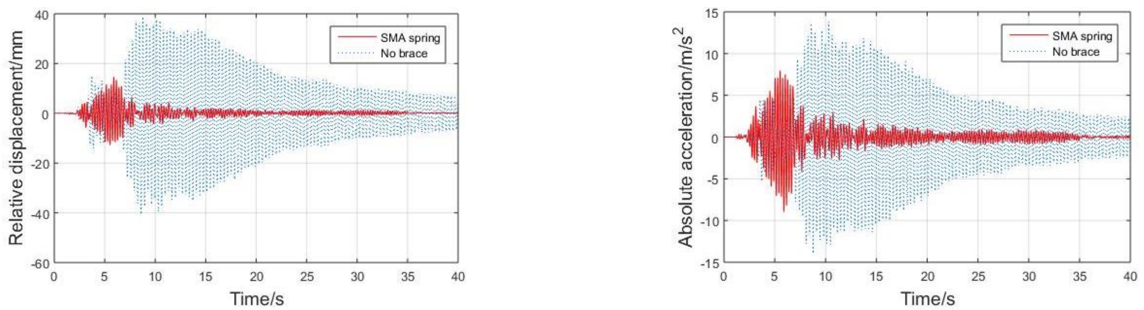

(a) Relative displacement (b) Absolute acceleration

Fig. 14 Response histories of the second-floor of the frame structure under the Kobe wave

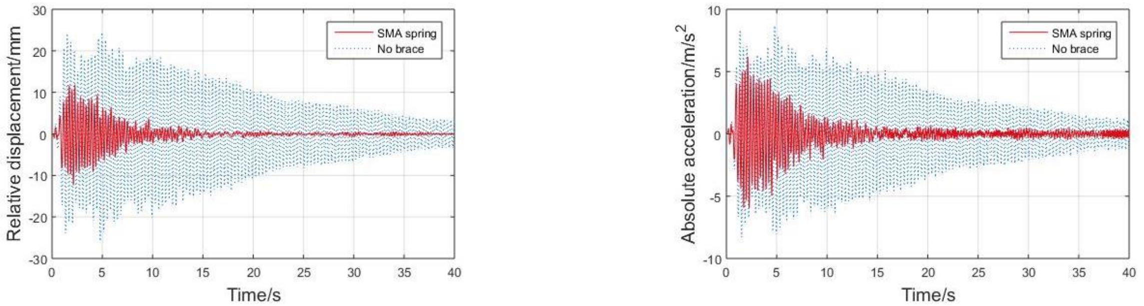

(a) Relative displacement (b) Absolute acceleration

Fig. 15 Response histories of the second-floor of the frame structure under the Hollister wave

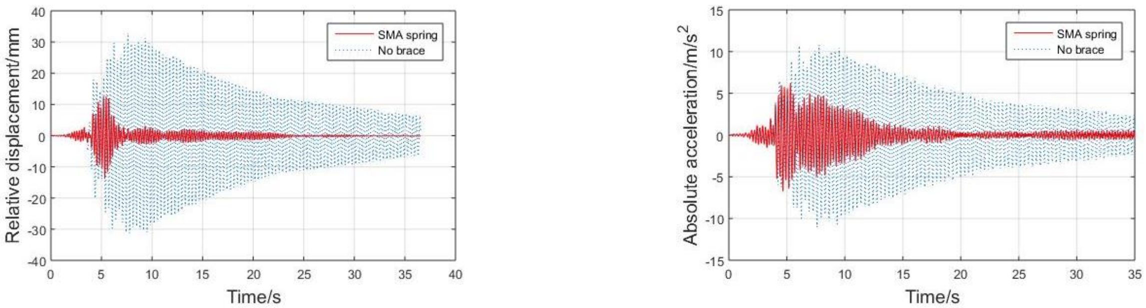

(a) Relative displacement (b) Absolute acceleration

Fig. 15 Response histories of the second-floor of the frame structure under the Hollister wave with/without SMA braces are plotted in Figs. 14-16. These responses consist of the relative displacement and the absolute acceleration. According to Figs. 14-16, regardless of the relative displacement or the absolute acceleration, the vibration reduction effects of the SMA spring braces are substantial. Hence, the optimization of the parameters of the SMA spring braces is highly useful for improving the seismic resistance of the frame.

6. Conclusions

This paper conducts a parametric study of SMA spring braces for providing seismic resistance of the frame structure. To implement this study, four SMA springs are fabricated and their force-displacement relationships are evaluated via tension tests. A two-floor steel frame is constructed and the performance of a numerical dynamic model of the frame structure system is evaluated via a series of shaking table tests. Then, the influences of two spring parameters, namely, the ratio of the helical spring diameter to the wire diameter and the pre-stretch length, on the seismic responses of the frame structure are investigated.

The numerical and experimental results demonstrate that when the ratio of the helical spring diameter to the wire diameter of SMA spring is equal to 8, the reduction ratios of the seismic responses of the frame are the largest among the Type I, Type II, Type III and Type IV springs. Under the Kobe wave, the reduction ratios of the peak absolute accelerations and peak relative displacements exceed 40% and 60%, respectively. Moreover, the peak absolute accelerations and the peak relative displacements of the frame structure can be reduced simultaneously for three types of earthquake waves when the optimal spring parameters are utilized.

Among the four types of manufactured SMA springs, the optimal pre-stretch lengths differ. For instance, one optimal length is 30 mm and another is 70 mm. However, for different SMA springs, if the pre-stretch length is assigned a reasonable value, excellent vibration reduction performance can be realized. It is highly important to select SMA spring braces with optimal parameters for minimizing the seismic responses of frame structures under various earthquake waves. Further it is expected that the large SMA springs can be made for the vibration reduction of the large scale structures in the future.

Acknowledgments

The authors would like to acknowledge financial support from the National Natural Science Foundation of China (Project No. 51578431).

References

Aguiar, R.A.A., Savi, M.A. and Pacheco, P.M.C.L. (2010), "Experimental and numerical investigations of shape memory alloy helical springs", *Smart Mater. Struct.*, **19**(2). https://doi.org/10.1088/0964-1726/19/2/025008

An, Y.H., Jo, H.K., Spencer Jr., B.F. and Ou, J.P. (2014), "A damage localization method based on the 'jerk energy'", *Smart Mater. Struct*., **23**(2). https://doi.org/10.1088/0964-1726/23/2/025020

Bae, J.S., Kwak, M.K. and Inman, D.J. (2005), "Vibration suppression of a cantilever beam using eddy current damper", *J. Sound Vib.*, **284**(3-5), 805-824. https://doi.org/10.1016/j.jsv.2004.07.031

Boyd, J.G. and Lagoudas, D.C. (1996), "A thermodynamical constitutive model for shape memory materials: part I. The monolithic shape memory alloy", *Int. J. Plasticity*, **12**(6), 805-842. https://doi.org/10.1016/S0749-6419(96)00030-7

Carreras, G., Casciati, F. and Casciati, S. (2010), "Fatigue laboratory tests toward the design of SMA portico-braces", *Smart Struct. Syst., Int. J*., **7**(1), 41-57. https://doi.org/ 10.12989/sss.2011.7.1.041

Casciati, F. and Faravelli, L. (2009), "A passive control device with SMA components: from the prototype to the model", *Struct. Control Hlth.*, **16**(7-8), 751-765. https://doi.org/10.1002/stc.328

Casciati, F. and van der Eijk, C. (2008), "Variability in mechanical properities and microstructure characterization of CuAlBe shape memory alloys for vibration mitigation", *Smart Struct. Syst., Int. J.*, **4**(2), 103-121. https://doi.org/103-121,10.12989/sss.2008.4.2.103

Casciati, F. and Wu, L.J. (2012), "Local positioning accuracy of laser sensors for structural health monitoring", *Struct. Control Hlth.*, **20**(5), 728-739. https://doi.org/10.1002/stc.1488

Casciati, F., Faravelli, L. and Hamdaoui, K. (2007), "Performance of a base isolator with shape memory alloy bars", *Earthq. Eng. Eng. Vib.*, **6**(4), 401-408. https://doi.org/10.1007/s11803-007-0787-2

Casciati, S. Faravelli, L. and Vece, M. (2016), "Investigation on the fatigue performance of Ni-Ti thin wires", *Struct. Control Health Monit*., **24**(1). https://doi.org/10.1002/stc.1855

De Domenico, D. and Ricciardi, G. (2018), "An enhanced base isolation system equipped with optimal tuned mass damper inerter (TMDI)", *Earthq. Eng. Struct. Dyn.*, **47**(5), 1169-1192. https://doi.org/10.1002/eqe.3011

Enemark, S., Santos, I.F. and Savi, M.A. (2016), "Modelling, characterisation and uncertainties of stabilised pseudoelastic shape memory alloy helical springs", *J. Intel. Mat. Syst. Struct.*, **27**(20), 2721-2743. https://doi.org/10.1177/1045389X16635845

Friedman, A.J., Dyke, S.J. and Phillips, B.M. (2013), "Over-driven control for large-scale MR dampers", *Smart Mater. Struct.*, **22**(4). https://doi.org/10.1088/0964-1726/22/4/045001

Gu, H. and Song, G.B. (2007), "Active vibration suppression of a flexible beam with piezoceramic patches using robust model reference control", *Smart Mater. Struct.*, **16**(4), 1453-1459. https://doi.org/10.1088/0964-1726/16/4/060

Hashemi, Y.M., Kadkhodaei, M. and Mohammadzadeh, M.R. (2019), "Fatigue analysis of shape memory alloy helical springs", *Int. J. Mech. Sci.*, **161**. https://doi.org/10.1016/j.ijmecsci.2019.105059

Hayashi, K., Skalomenos, K.A. and Inamasu, H. (2018), "Self-centering rocking composite frame using double-skin concrete-filled steel tube columns and energy-dissipating fuses in multiple locations", *J. Stuct. Eng.*, **144**(9). https://doi.org/10.1061/(ASCE)ST.1943-541X.0002157

Huang, B., Zhang H.Y. and Wang, H. (2014), "Passive base isolation with superelastic Nitinol SMA helical springs", *Smart Mater. Struct*., **23**(6). https://doi.org/10.1088/0964-1726/23/6/065009

Huang, Z.W., Hua, X.G. and Chen, Z.Q. (2018a), "Modeling, testing, and validation of an eddy current damper for structural vibration control", *J. Aerospace Eng.*, **31**(5). https://doi.org/10.1061/(ASCE)AS.1943-5525.0000891

Huang, B., Lao, Y.M. and Chen, J.M. (2018b), “Dynamic response analysis of a frame structure with superelastic nitinol SMA helical spring braces for vibration reduction”, *J. Aerosp. Eng.*, **31**(6). https://doi.org/10.1061/(asce)as.1943-5525.0000923

Huang, B., Lv, H.W. and Song, Y. (2019), “Numerical simulation and experimental study of a simplified force-displacement relationship in superelastic SMA helical springs”, *Sensors*, **19**(1). https://doi.org/10.3390/s19010050

Kim, J., Ryu, J. and Chung, L. (2006), “Seismic performance of structures connected by viscoelastic dampers”, *Eng. Struct.*, **28**(2), 183-195. https://doi.org/10.1016/j.engstruct.2005.05.014

Kundu, P., Nath, T. and Palani, I.A. (2018), “Integrating GLL-Weibull distribution within a Bayesian framework for life prediction of shape memory alloy spring undergoing thermo-mechanical fatigue”, *J. Mater. Eng. Perform*, **27**(7). https://doi.org/10.1007/s11665-018-3435-2

Mishra, S.K., Gur, S. and Chakraborty, S. (2013), “An improved tuned mass damper (SMA-TMD) assisted by a shape memory alloy spring”, *Smart Mater. Struct.*, **22**(9). https://doi.org/10.1088/0964-1726/22/9/095016

Motahari, S.A. and Ghassemieh, M. (2007), “Multilinear one-dimensional shape memory material model for use in structural engineering applications”, *Eng. Struct.*, **29**(6), 904-913. https://doi.org/10.1016/j.engstruct.2006.06.007

Patil, D. and Song, G.B. (2016), “Shape memory alloy actuated accumulator for ultra-deepwater oil and gas exploration”, *Smart Mater. Struct.*, **25**. https://doi.org/10.1088/0964-1726/25/4/045012

Qian, H., Li, H.N. and Song, G.B. (2016), “Experimental investigations of building structure with a superelastic shape memory alloy friction damper subject to seismic loads”, *Smart Mater. Struct.*, **25**(12). https://doi.org/10.1088/0964-1726/25/12/125026

Ren, W.X., Li, H.N. and Song, G.B. (2007), “A one-dimensional strain-rate-dependent constitutive model for superelastic shape memory alloys”, *Smart Mater. Struct*, **16**(1), 191-197. https://doi.org/10.1088/0964-1726/16/1/023

Saadat, S., Salichs, J. and Noori, M. (2002), “An overview of vibration and seismic applications of NiTi shape memory alloy”, *Smart Mater. Struct.*, **11**(2), 218-229. https://doi.org/0964-1726/11/2/305

Sedlák, P., Frost, M. and Kruisová, A. (2014), “Simulations of mechanical response of superelastic NiTi helical spring and its relation to fatigue resistance”, *J. Mater. Eng. Perform.*, **23**(7), 2591-2598. https://doi.org/10.1007/s11665-014-0906-y

Song, G., Ma, N. and Penny, N. (2004), “Design and control of a proof-of-concept active jet engine intake using shape memory alloy actuators”, *Smart. Struct. Syst., Int. J.*, **7**(1), 1-13. https://doi.org/10.1088/0964-1726/16/4/048

Song, G., Ma, N. and Li, H.N. (2006a), “Applications of shape memory alloys in civil structures”, *Eng. Struct.*, **28**(9), 1266-1274. https://doi.org/10.1016/j.engstruct.2005.12.010

Song, G., Mo, Y.L. and Otero, K. (2006b), “Health monitoring and rehabilitation of a concrete structure using intelligent materials”, *Smart Mater. Struct.*, **15**(2), 309-314. https://doi.org/10.1088/0964-1726/15/2/010

Sun, W.Q. (2011), “Seismic response control of high arch dams including contraction joint using nonlinear super-elastic SMA damper”, *Constr. Build. Mater.*, **25**(9), 3762-3767. https://doi.org/10.1016/j.conbuildmat.2011.04.013

Wang, W.X., Hua, X.G. and Wang, X.Y. (2018a), “Numerical modeling and experimental study on a novel pounding tuned mass damper”, *J. Vib. Control*, **24**(17). https://doi.org/10.1177/1077546317718714

Wang, W.X., Wang, X.Y. and Hua, X.G. (2018b), “Vibration control of vortex-induced vibrations of a bridge deck by a single-side pounding tuned mass damper”, *Eng. Struct.*, **173**, 61-75. https://doi.org/10.1016/j.engstruct.2018.06.099

Wang, S.J., Chiu, I.C. and Yu, C.H. (2019), “Experimental beyond design and residual performances of full-scale viscoelastic dampers and their empirical modeling”, *Earthq. Eng. Struct. Dyn.*, **48**(10), 1093-1111. https://doi.org/10.1002/eqe.3170

Xu, M.B. and Song, G. (2004), “Adaptive control of vibration wave propagation in cylindrical shells using SMA wall joint”, *J. Sound Vib.*, **278**(1-2), 307-326. https://doi.org/10.1016/j.jsv.2003.10.029

Yang, Q.S., Lu, X.Z. and Yu, C. (2017), “Experimental study and finite element analysis of energy dissipating outriggers”, *Adv. Struct. Eng.*, **20**(8), 1196-1209. https://doi.org/10.1177/1369433216677122

Yoshida, O. and Dyke, S.J. (2004), “Seismic control of a nonlinear benchmark building using smart dampers”, *J. Eng. Mech.*, **130**(4), 386-392. https://doi.org/10.1061/(ASCE)0733-9399(2004)130:4(386)

Zapateiro, M., Karimi, H.R. and Luo, N. (2009), “Real-time hybrid testing of semiactive control strategies for vibration reduction in a structure with MR damper”, *Struct. Control Health*, **17**(4), 427-451. https://doi.org/10.1002/stc.321

Zhang, P., Song, G. and Li, H.N. (2012), “Seismic control of power transmission tower using pounding TMD”, *J. Eng. Mech.-ASCE*, **139**(10), 1395-1406. https://doi.org/10.1061/(ASCE)EM.1943-7889.0000576

Zhou, H., Li, J. and Spencer Jr., B.F. (2019), “Multiscale random fields-based damage modeling and analysis of concrete structures”, *J. Eng. Mech*., **145**(7). https://doi.org/10.1061/(ASCE)EM.1943-7889.0001618

BS